This is the peer reviewed version of the following article: Surface-Assisted Cyclodehydrogenation; Break the Symmetry, Enhance the Selectivity Chem. Eur. J., volume 21, pages 12285–12290, year 2015, which has been published in final form at DOI: 10.1002/chem.201502001. This article may be used for non-commercial purposes in accordance with Wiley Terms and Conditions for Self-Archiving.

Alissa Wiengarten,[1] Julian A. Lloyd,[1] Knud Seufert,[1] Joachim Reichert,[1, a)] Willi Auwärter,[1] David A. Duncan,[1] Francesco Allegretti,[1] Sybille Fischer,[1] Seung Cheol Oh,[1] Özge Sağlam,[1] Li Jiang,[1] Saranyan Vijayaraghavan,[1] David Écija,[1] Anthoula C. Papageorgiou,[1, b)] and Johannes V. Barth[1]
Physik Department E20, Technische Universität München, 85748 Garching, Germany

Selectivity in chemical reactions is a major objective in industrial processes to minimize spurious byproducts and to save scarce resources. In homogeneous catalysis the most important factor which determines selectivity is structural symmetry. However, a transfer of the symmetry concept to heterogeneous catalysis still requires a detailed comprehension of the underlying processes. Here, we investigate a ring-closing reaction in surface-confined *meso*-substituted porphyrin molecules by scanning tunneling microscopy, temperature-programmed desorption, and computational modeling. The identification of reaction intermediates enables us to analyze the reaction pathway and to conclude that the symmetry of the porphyrin core is of pivotal importance regarding product yields.

Keywords: heterogeneous catalysis, porphyrins, ring-closing reaction, selectivity, symmetry

Selectivity in surface chemical reactions is of paramount importance in the development of future catalysts and devices.[1] Not only does selectivity have a substantial impact on the efficiency of a given process, it also leads to reduced yields of spurious byproducts.[1c,2] Although bond-selective chemical transformations can be achieved through photocatalysis[3] or singlemolecule experiments using scanning tunneling microscopy (STM),[4] by far the leading driver of selectivity is structural symmetry.[5] Most notably, structural symmetry is crucial in biological processes[6] and large-scale production of fine chemicals,[7] including synthesis routes to both organic and inorganic compounds,[8] especially by homogeneous catalysis.[9] However, bestowing selectivity on solid surfaces, that is, extension to heterogeneous catalysis, is still largely in its infancy though it is a field that has attracted a great deal of attention.[1c,10] Parameters that can drive selectivity in on-surface chemistry comprise surface reactivity[11] and structure,[12] as well as the molecular geometry.[13]

Cyclodehydrogenation reactions are currently employed in the on-surface syntheses of fullerenes,[14] graphene nanoribbons,[13c] tailored nanographenes[13b] as well as carbon nanotubes.[15] So far the possibility to steer selectivity into this class of surface-assisted reactions has not been explored. Here, we study a cyclodehydrogenation or ring-closing reaction, with a selective[1a] outcome which is determined by the intrinsic symmetry of the molecule (Scheme 1).

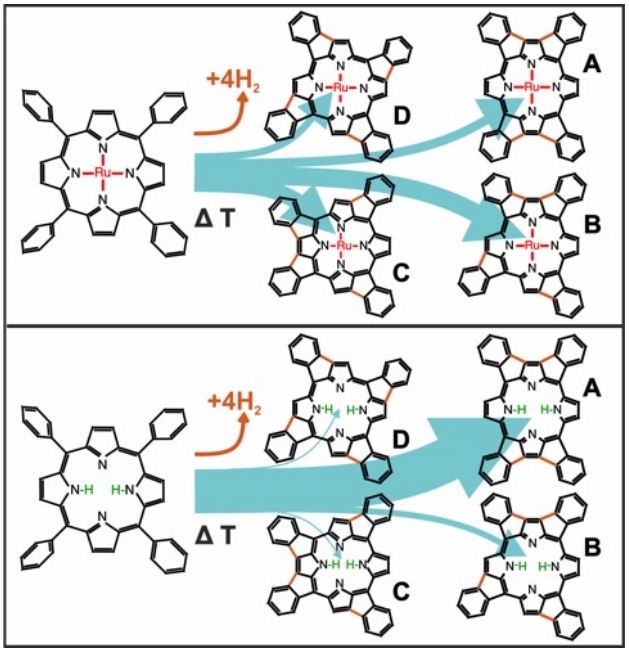

FIG. 1. *
Scheme 1. Dehydrogenative ring-closing reactions for a Ru-tetraphenyl-porphyrin (Ru-TPP) (top) and a 2H-tetraphenyl-porphyrin (2H-TPP) (bottom) with markedly different product yields as indicated for adsorbed species.

Ring-closing and -fusing reactions on porphyrins are well-studied in solution,[16] however as reported recently,[17] free-base tetraphenylporphyrin (2H-TPP) molecules undergo several cyclodehydrogenation reactions upon annealing on a Ag(111) surface (Scheme

a) Electronic mail: joachim.reichert@tum.de
b) Electronic mail: a.c.papageorgiou@tum.de

1, bottom). In solution, this type of fusion of a *meso* substituent and the porphyrin periphery is usually metal-catalyzed, for example, for *meso*-linked dibenzo[*a,g*]corannulene- porphyrin it is mediated by $FeCl_3$ at room temperature (RT).[18] Although four different reaction products could be identified by STM, the formation of a specific species (**A** in Scheme 1) is clearly favored.[16a,17b] By solution synthesis, the Zn-metalated species **A** can be obtained from a Zn-TPPBr_4 precursor molecule, brominated at the appropriate positions of the porphyrin periphery.[16a] Hitherto this selectivity has not been addressed explicitly and has often been misidentified.[17a,19] With submolecular resolution of STM, we identify reaction intermediates providing a direct insight into the reaction pathway. Comparison with density functional theory (DFT) calculations of the ground state energies of the reaction intermediates indicates that the twofold symmetry of the 2H-TPPs core, which is defined by the position of the H atoms, determines the reaction outcome. To substantiate this interpretation, related Ru-TPP species (Scheme 1) with a fourfold core, are subjected to a similar treatment. Indeed, the higher symmetry entails a significant decrease in the selectivity of the ring-closing reactions.

Room-temperature deposition of either Ru-TPP or 2H-TPP molecules onto a Ag(111) substrate leads to the formation of extended islands (see Figure 1a and c, a single Ru-TPP and a single 2H-TPP are outlined in red and green, respectively).[20] The molecules form a dense-packed layer stabilized by T-type interactions between the terminal phenyl groups.[20,21] Annealing 2H-TPP molecules to temperatures between 530 K and 620 K for 10 min induces dehydrogenation reactions and the formation of C−C bonds between the phenyl rings and the macrocycle resulting in planar porphyrin derivatives (PPDs, see Figure 1d and Scheme 1).[17] Consequently, the phenyl rings can no longer interact via T-type interaction and thus regular islands of PPDs are not observed. Otherwise, intermolecular distances at low coverages imply no long-range repulsive interaction between the molecules (see Figure S1). Upon annealing Ru-TPP molecules to 620 K the same ring-closing reactions as described for the 2H-TPP molecules take place. Four different PPDs are observed in high-resolution STM images (see Figure 1b and Figure S2) and the tentative structural models are shown in Scheme 1.

However, the occurrence of the four reaction products is very different for both molecules, as can be seen in Figure 1e, where the respective occurrence of all four species (**A** to **D**) is shown. For Ru-TPP, species **B** and **C** amount to slightly more than 30% each and species **A** and **D** to less than 20% each. On the contrary, the reaction is very selective for 2H-TPP, where 86% of the PPDs appear as species **A**, only 12% as species **B** and less than 3% as **C** or **D**.

The bright features in Figure 1d (one such feature marked by a black circle) are attributed to partially flattened molecules. As will be shown below, such intermediate species with some upstanding (unreacted) and some planar (reacted) phenyl rings are observed where the former show a larger apparent height than the latter.

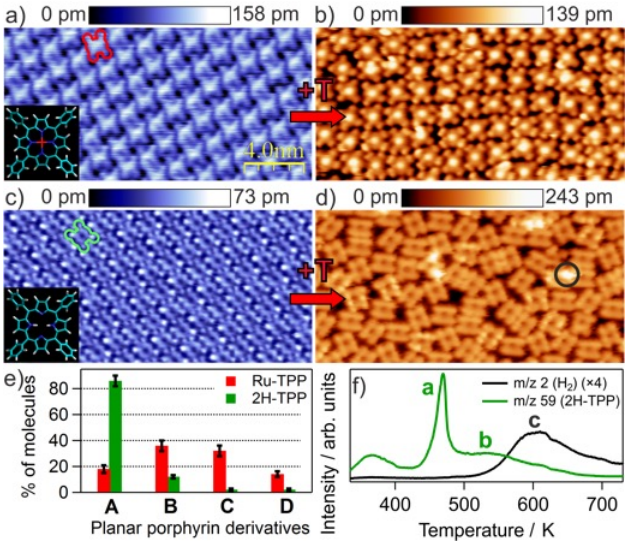

FIG. 1. STM images, product distributions and TPD spectra of Ru-TPP and 2H-TPP and their respective cyclodehydrogenation products on Ag(111). a) A monolayer of Ru-TPP molecules after room-temperature (RT) deposition, inset: structural model of Ru-TPP (C, N, Ru, and H atoms are indicated in cyan, blue, red, and white, respectively). b) Planar Ru-porphyrin derivatives after annealing the surface shown in (a) to 620 K for 10 min, a) and b) imaged at RT, molecules stabilized by high coverage. c) a monolayer of 2H-TPP molecules after RT deposition, inset: structural model of 2H-TPP. d) Planar porphyrin derivatives after annealing the surface shown in (c) to 560 K for 10 min, c) and d) imaged at 6 K. e) Histogram of different planar porphyrin derivatives for Ru-TPP (red) and 2H-TPP (green) molecules (for labels **A** to **D** see Scheme 1). Several hundred molecules were sampled for both histograms. f) TPD spectra measured from a multilayer coverage of 2H-TPP molecules showing dehydrogenation (black line) and molecular desorption (green line: *m/z* 59, indicative of 2H-TPP desorption) at a heating rate of 0.5 Ks^{-1}. [a) 1.4 V, 0.06 nA, b) −1.2 V, 0.05 nA, c) −0.8 V, 0.2 nA, d) −0.3 V, 0.1 nA].

Annealing to temperatures above 670 K leads to polymerization reactions between the molecules by C−H activation and formation of new intermolecular C−C bonds (see Figure S3), similar to the homocoupling of porphine molecules on Ag(111).[22]

To assess the proposed dehydrogenation and to determine its onset temperature, temperature-programmed desorption (TPD) experiments were carried out monitoring the desorption of both 2H-TPP and hydrogen molecules. In Figure 1f the TPD spectrum for *m/z* (mass-to-charge ratio) 59, a fragment of the unreacted molecule, with a heating rate of 0.5 Ks^{-1} shows a pronounced peak at 470 K (a) with an onset at $\sim$ 450 K and a broad feature (b) extending over the range in which flattening occurs (see also Figure S7). Peak (a) is as-

signed to the desorption of the multilayer, which leaves behind a densely packed monolayer, and although it is not clear whether the latter feature (b) relates entirely to the flattening, clearly some of the densely packed monolayer must desorb during this process, as the product species have larger surface footprints than the unreacted 2H-TPP (by $\sim 11\%$ based on the highest packing densities observed by STM). On the other hand, the H_2 TPD spectrum displays a dominant peak (c) which extends over a broad temperature range and has its onset at ~ 500 K, a value that agrees well with the temperature at which the flattening is observed by STM. Note that a shoulder is present at higher temperatures, however as shown in Figure S8 in the Supporting Information, this desorption feature seems to have a higher reaction order than the H_2 originating from the flattening process, as implied by its variance in temperature as a function of coverage. This suggests that this shoulder is related to the release of H_2 resulting from polymerization of flattened 2H-TPP (Figure S3). One has to mention here that it is known from X-ray photoelectron spectroscopy (XPS) that the central nitrogen atoms do not dehydrogenate upon annealing at ~ 550 K.[17]

Considering that the TPD experiments indicate an onset temperature for the cyclodehydrogenation reaction of ~ 500 K, a multilayer of 2H-TPP molecules on Ag(111) was annealed to 520 K for 10 min. After subsequent cooling to 6 K different molecular species can be observed. About one fifth of the molecules appear as unreacted 2H-TPP molecules (Figure 2a), an even smaller amount is completely flat on the surface (Figure 3, bottom panel). The rest of the molecules are partially flattened (Figure 2b–d), the upstanding phenyl rings are evident in the STM images by their higher apparent height (see line profile in Figure S4). Thus, we can conclude that the reaction proceeds in multiple steps, affording reaction intermediates.

In general, the probability to undergo a chemical reaction is mainly dependent on its reaction barrier rather than the energetic difference between the reactant and the product. However, based on the following arguments, we rationalize the reaction pathway by DFT ground state calculations of isolated species. Since the reaction takes place at elevated temperatures, where a portion of the molecules desorbs and the interaction with the surface is substantially weakened, a situation which is poorly described by DFT simulations at 0 K, we chose to conduct these simulations without any supporting substrate. As the reactions are all very similardehydrogenation and C−C bond formationit can be assumed that the activation energy is inversely linked to the enthalpy of the reaction that is released (Bell–Evans–Polanyi principle).[23] Consequently, the reaction with the highest enthalpy of reaction occurs also with the highest rate. This allows the reaction pathway to be assessed by calculating the ground state energies of the potential products (see Figure 3).

In the following, all intermediate species observed by

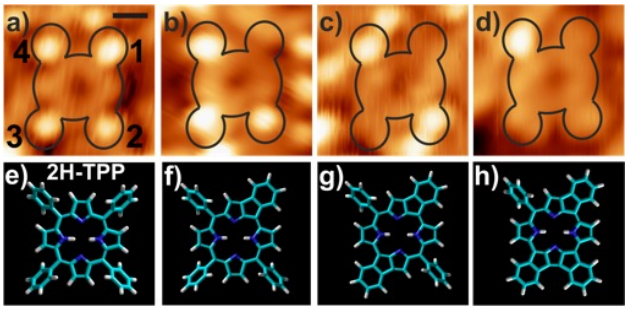

FIG. 2. High-resolution STM data of partially flattened porphyrin molecules with structural models. a) Unreacted 2H-TPP (scale bar 5 Å), b) intermediate species type 1 (RI1) with one flat phenyl ring, c) intermediate species type 2 (RI2) with two flat phenyl rings, d) intermediate species type 3 (RI3) with three flat phenyl rings. The outlines of the molecules are marked with a black line. e) Structural model of the 2H-TPP molecule. f) to h) Tentative structural models of RI1-3. [STM images recorded at 6 K. a) −1 V, 0.2 nA, b) −0.5 V, 0.2 nA, c) −1 V, 0.2 nA, d) −0.5 V, 0.2 nA].

STM will be compared to the ground state energies calculated for different possible intermediates. Figure 2a shows an STM image of an unreacted 2H-TPP molecule where the four bright lobes are assigned to the four phenyl rings that are rotated out of the surface plane and therefore show a larger apparent height than the macrocycle which lies parallel to the surface and appears with a depression in the center.

The first reaction intermediate species type 1 (RI1) (Figure 2b) exhibits a similar appearance of the macrocycle but with only three bright lobes. At the position of the first phenyl ring (see Figure 2a) the apparent height is similar to that of the macrocycle, that is, a ring-closing reaction took place and an additional C−C bond with the macrocycle formed. A structural model of RI1 is given in Figure 2f, however it has to be emphasized that it is not possible to distinguish in the STM images with which macrocyclic moiety the first phenyl ring has reacted, the pyrrolic (−NH) or the iminic one (= N). Compounds **1** and **2** in the first block of Figure 3 are the two possibilities for this first ring-closing reaction, corresponding to RI1. Compound **2** is found to have the lowest ground state energy (indicated by the white background) with **1** having a higher ground state energy by 0.074 eV.

In the subsequent steps only reaction pathways which include the reaction intermediates with the lowest ground state energy are considered. Thus, starting from **2** there are six different possibilities for the flattening of the second phenyl ring (**3** to **8**). Compound **6** is found to have the lowest ground state energy and **4** exhibits only a very small energy difference. In the STM images **5** and **6** cannot be differentiated but, if the molecules are not too close to each other, they can be differentiated from **3**, **4**, **7**, and **8** (see Figure S5). In the STM images **5** and/or **6** make up the majority of RI2 (Figure 2c).

Starting from **6** there are two possibilities for the third

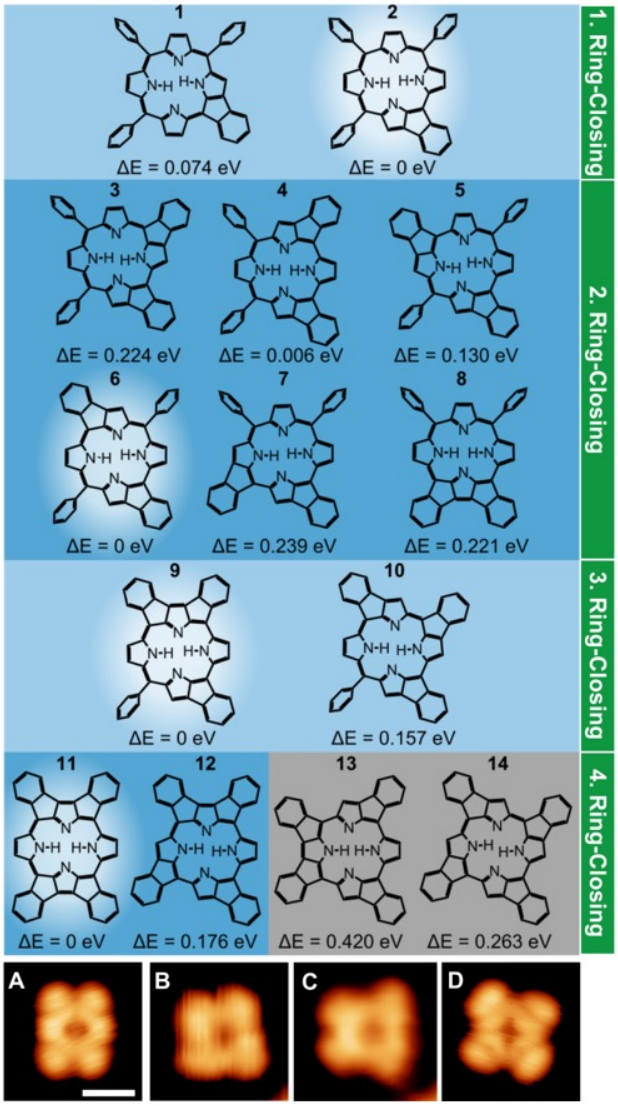

FIG. 3. Ground-state energies, calculated using DFT, explain the proposed reaction pathway of the stepwise flattening. Each step (excluding **13** and **14**) starts with the energetically most favored structure of the step before. **1** and **2**: First ring-closing, **3** to **8**: second ring-closing, **9** and **10**: third ring-closing, **11** to **14**: four planar porphyrin derivatives which were observed by STM with respective STM images below (**A** to **D**). ΔE is calculated with respect to the lowest ground state energy of each reaction step (respective compound highlighted by white background). The scale bar in **A** indicates 1 nm. [STM images recorded at 6 K. **A**: −0.01 V, 0.1 nA, **B**: −0.8 V, 0.2 nA, **C**: −0.8 V, 0.2 nA, **D**: −0.01 V, 0.1 nA].

ring-closing reaction. The species with the lowest ground state energy (**9**) is also the most frequently observed RI3 species in the STM measurements (see Figure 2d). A smaller amount appears as **10** and different configurations resulting from other RI2 than **6** are observed (see Figure S5).

The last row of models in Figure 3 shows the four PPDs which are resolved in our STM measurements (presented below the models).[17b] After the formation of **9**, the only two possibilities for the final ring-closing reaction are **11** and **12**, with **11** being significantly more favorable. This is in good agreement with the selectivity observed in the STM measurements since the majority of all PPDs (86%) appears as **A** and only a small fraction (12%) as **B**. On the other hand, this implies that at least 14% of the molecules did not convert into the energetically favored intermediate and/or product in all steps. From our measurements and calculations it is not possible to infer in which step of the reaction a reaction intermediate with $\Delta E > 0$ is formed.

Please note that tautomerization of the reaction intermediates may play an important role for the selectivity of the reaction pathway. It is known that the central hydrogens can tautomerize,[24] for example, **1** is the tautomer of **2**. Nevertheless, the former degeneracy of this tautomerization in the pristine 2H-TPP molecule is lifted after the first ring-closing reaction and the ratio between the tautomers is certainly shifted towards the energetically more stable tautomer (**2**).

Judging from the appearance in the STM images, the two central hydrogen atoms in species **A** are bound to the unreacted pyrrole rings. Furthermore, no tautomerization of the PPDs could be observed after voltage pulses by the tip (cf. ref. [24b] where tautomerization was observed for 2H-TPP molecules under the same conditions), that is, either the tautomers cannot be distinguished by STM or tautomerization does not occur. This assumption is corroborated by the DFT calculations. The energetic difference between the tautomers is significantly increased after the fourth ring-closing in comparison to the first ring-closing. The ground state energy of the tautomer of **11** is 0.55 eV higher, suggesting that the tautomerization of the PPDs is suppressed.

Remarkably, the prevailing reaction product is the same for calculations and experiment, despite the DFT modeling is based on stark simplifications, namely the comparison of only ground state energies for intermediates and products as well as the absence of a substrate. This may imply that the origin of the selectivity for the reaction is related to the molecule itself rather than to surface interactions. As described above, the occurrence of the four different reaction products is markedly different for the case of Ru-TPP (see Figure 1e), where no specific product is favored. Furthermore, our preliminary investigations on another metalloporphyrin, the Co-TPP, show a similar distribution of products for the same flattening reaction as in the case of Ru-TPP. Moreover, our annealing experiments with a slightly different molecule, namely the 5,15-diphenylporphyrin, support the suggested reaction pathway. The two ring-closing reactions for the majority of the molecules, which occur upon annealing, provide preferentially a flat species similar to **6** for 91% of the molecules on a Ag(111) (see Figure S6) as well as on a Ag(100) surface. This supports our assumption for the DFT calculations that the surface has

only a minor impact on the selectivity of the reaction. In addition, with these similar results for two different metalloporphyrins and two free-base porphyrins, an influence of the symmetry of the core of the molecule on the selectivity of the reaction can be anticipated.

In conclusion, we presented a systematic study regarding symmetry-driven surface chemical transformations. For the exemplary case of surface-assisted cyclodehydrogenation reactions of related *meso*-substituted free-base versus metalloporpyhrins, we find that the twofold symmetry of the 2H-TPPs core, imposed by the two central hydrogens, drives the selectivity of a reaction at the periphery of the molecule towards a distinct product. Such selectivity could not be observed when triggering the same ring-closing reaction in Ru-TPP or Co-TPP species, where macrocycle core has a fourfold symmetry. Based on this model case, we expect that ab initio calculations of the energetically favored products can provide valuable guidelines for the outcome of surface-assisted cyclodehydrogenation reactions. These insights contribute towards the targeted design of molecular precursors for the engineering of conjugated nanostructures by on-surface synthesis and advanced porphyrin-based architectures at interfaces.[25]

EXPERIMENTAL SECTION

The Ag(111) substrate was prepared by repeated cycles of Ar^+ sputtering and annealing to 720 K. 2H-TPP (Sigma-Aldrich, $\geq 99\%$) and Ru(CO)-TPP (Sigma-Aldrich, $\sim 80\%$) molecules were thoroughly outgassed in ultrahigh vacuum (UHV) and deposited by organic molecular beam epitaxy (OMBE) from quartz crucibles held at 575–590 K and at ~ 613 K, respectively. The temperature during annealing experiments and STM measurements was monitored by a type K thermocouple directly attached to the Ag(111) single crystal. The STM experiments were carried out in two UHV systems: First, in a custom-designed UHV system with a low temperature CreaTec- STM at a base pressure $< 8 \times 10^{-10}$ mbar (scanning temperature 6 K). Second, in a home-made UHV chamber equipped with an Aarhus-type variable-temperature STM at a base pressure $< 2 \times 10^{-10}$ mbar (scanning temperature 300 K). In both cases, the STM images were acquired in constant current mode with chemically etched W tips and processed with WSxM.[26] The bias voltage of the tunneling parameters refers to the voltage applied to the sample. The TPD experiments were performed in a separate custom-built UHV system using a liquid nitrogen cooled quadrupole mass spectrometer with a Feulner cup[27] that can be brought within a few millimeters of the sample. The heating rate was controlled by a proportional-integral-derivative controller and kept constant within $< \pm 0.1$ Ks^{-1}. The pressure during TPD measurements was between 2 to $< 8 \times 10^{-11}$ mbar and typically the background pressure of H_2 was on the detection limit of the mass spectrometer before TPD measurements began. The cleanliness of the Ag(111) substrate and the evaporated molecules was assessed using XPS; however, due to observed beam damage to the 2H-TPP multilayer, XPS was not performed prior to TPD measurements. TPD control experiments are presented in the Supporting Information. DFT calculations were performed using the Gaussian Software package.[28] Using the 6–311G basis in combination with Perdew-Burke-Ernzerhof[29] exchange and correlation functionals, the different molecular structures were optimized towards the lowest possible ground state energy. Calculations were performed on single molecules in the gas phase using the default convergence criteria of the program.

ACKNOWLEDGMENTS

This work was supported by the ERC Advanced Grant MolArt (No. 247299), the Munich Center for Advanced Photonics (MAP), and the Technische Universität München-Institute for Advanced Study, funded by the German Research Foundation (DFG) via the German Excellence Initiative. A.W., D.A.D., Ö.S., L.J., and A.C.P. were supported by the International Max Planck Research School of Advanced Photon Science, the Alexander von Humboldt Foundation, a Marie Curie International Incoming Fellowship (Project NANOULOP, No. 302157), the China Scholarship Council, and a Marie Curie Intra-European Fellowship (project NASUMECA, No. 274842), respectively. We thank Peter Feulner, Carlos-Andres Palma and Ari P. Seitsonen for helpful discussions.

Supporting information for this article is available on the WWW under http://dx.doi.org/10.1002/chem.201502001.

REFERENCES AND NOTES

1. a) B. M. Trost, *Science* **1983**, *219*, 245–250; b) J. Grunes, J. Zhu, G. A. Somorjai, *Chem. Commun.* **2003**, 2257–2260; c) G. A. Somorjai, J. Y. Park, *Angew. Chem. Int. Ed.* **2008**, *47*, 9212–9228.

2. P. Anastas, N. Eghbali, *Chem. Soc. Rev.* **2010**, *39*, 301–312.

3. a) A. Sinha, M. C. Hsiao, F. F. Crim, *J. Chem. Phys.* **1991**, *94*, 4928–4935; b) M. Dantus, V. V. Lozovoy, *Chem. Rev.* **2004**, *104*, 1813–1860; c) A. Assion, T. Baumert, M. Bergt, T. Brixner, B. Kiefer, V. Seyfried, M. Strehle, G. Gerber, *Science* **1998**, *282*, 919–922.

4. a) B. C. Stipe, M. A. Rezaei, W. Ho, S. Gao, M. Persson, B. I. Lundqvist, *Phys. Rev. Lett.* **1997**, *78*, 4410–4413; b) S.-W. Hla, K.-H. Rieder, *Annu. Rev. Phys. Chem.* **2003**, *54*, 307–330; c) Y. Jiang, Q. Huan, L. Fabris, G. C. Bazan, W. Ho, *Nat. Chem.* **2012**, *5*, 36–41; d) J. I. Pascual, N. Lorente, Z. Song, H. Conrad, H. P. Rust, *Nature* **2003**, *423*, 525–528.

5. a) B. Smit, T. L. M. Maesen, *Nature* **2008**, *451*, 671–678; b) T. F. Degnan Jr., *J. Catal.* **2003**, *216*, 32–46.

6. A. Warmflash, B. Sorre, F. Etoc, E. D. Siggia, A. H. Brivanlou, *Nat. Methods* **2014**, *11*, 847–854.

7. a) H.-U. Blaser, B. Pugin, F. Spindler, *J. Mol. Catal. A* **2005**, *231*, 1–20; b) P. Etayo, A. Vidal-Ferran, *Chem. Soc. Rev.* **2013**, *42*, 728–754.

8. a) P. Linnane, N. Magnus, P. Magnus, *Nature* **1997**, *385*, 799–801; b) A. Lennartson, S. Olsson, J. Sundberg, M. Hakansson, *Angew. Chem. Int. Ed.* **2009**, *48*, 3137–3140; c) R. L. Halterman, S. T. Jan, *J. Org. Chem.* **1991**, *56*, 5253–5254.

9. a) O. I. Kolodiazhnyi, *Tetrahedron* **2003**, *59*, 5953–6018; b) K. Gopalaiah, *Chem. Rev.* **2013**, *113*, 3248–3296.

10. a) M. Heitbaum, F. Glorius, I. Escher, *Angew. Chem. Int. Ed.* 2006, *45*, 4732–4762; b) G. Kyriakou, S. K. Beaumont, R. M. Lambert, *Langmuir* **2011**, *27*, 9687–9695; c) A. Baiker, *J. Mol. Catal. A* **1997**, *115*, 473–493.

11. A. L. Pinardi, G. Otero-Irurueta, I. Palacio, J. I. Martinez, C. Sanchez-Sanchez, M. Tello, C. Rogero, A. Cossaro, A. Preobrajenski, B. Gomez-Lor, A. Jancarik, I. G. Stará, I. Starý, M. F. Lopez, J. Méndez, J. A. Martin-Gago, *ACS Nano* **2013**, *7*, 3676–3684.

12. H. Walch, R. Gutzler, T. Sirtl, G. Eder, M. Lackinger, *J. Phys. Chem. C* **2010**, *114*, 12604–12609.

13. a) A. Violi, *J. Phys. Chem. A* **2005**, *109*, 7781–7787; b) M. Treier, C. A. Pignedoli, T. Laino, R. Rieger, K. Müllen, D. Passerone, R. Fasel, *Nat. Chem.* **2011**, *3*, 61–67; c) J. Cai, P. Ruffieux, R. Jaafar, M. Bieri, T. Braun, S. Blankenburg, M. Muoth, A. P. Seitsonen, M. Saleh, X. Feng, K. Müllen, R. Fasel, *Nature* **2010**, *466*, 470–473; d) L. Grill, M. Dyer, L. Lafferentz, M. Persson, M. V. Peters, S. Hecht, *Nat. Nano* **2007**, *2*, 687–691.

14. G. Otero, G. Biddau, C. Sánchez-Sánchez, R. Caillard, M. F. López, C. Rogero, F. J. Palomares, N. Cabello, M. A. Basanta, J. Ortega, J. Méndez, A. M. Echavarren, R. Pérez, B. Gómez-Lor, J. A. Martín-Gago, *Nature* **2008**, *454*, 865–868.

15. J. R. Sanchez-Valencia, T. Dienel, O. Gröning, I. Shorubalko, A. Mueller, M. Jansen, K. Amsharov, P. Ruffieux, R. Fasel, *Nature* **2014**, *512*, 61–64.

16. a) T. Ishizuka, Y. Saegusa, Y. Shiota, K. Ohtake, K. Yoshizawa, T. Kojima, *Chem. Commun.* **2013**, *49*, 5939–5941; b) J. A. Faiz, V. Heitz, J.-P. Sauvage, *Chem. Soc. Rev.* **2009**, *38*, 422–442; c) N. K. S. Davis, A. L. Thompson, H. L. Anderson, *J. Am. Chem. Soc.* **2011**, *133*, 30–31.

17. a) G. Di Santo, S. Blankenburg, C. Castellarin-Cudia, M. Fanetti, P. Borghetti, L. Sangaletti, L. Floreano, A. Verdini, E. Magnano, F. Bondino, C. A. Pignedoli, M.-T. Nguyen, R. Gaspari, D. Passerone, A. Goldoni, *Chem. Eur. J.* **2011**, *17*, 14354–14359; b) A. C. Papageorgiou, S. Fischer, S. C. Oh, Ö. Sağlam, J. Reichert, A. Wiengarten, K. Seufert, S. Vijayaraghavan, D. Ecija, W. Auwärter, F. Allegretti, R. G. Acres, K. C. Prince, K. Diller, F. Klappenberger, J. V. Barth, *ACS Nano* **2013**, *7*, 4520–4526.

18. K. Ota, T. Tanaka, A. Osuka, *Org. Lett.* **2014**, *16*, 2974–2977.

19. M. Röckert, M. Franke, Q. Tariq, S. Ditze, M. Stark, P. Uffinger, D. Wechsler, U. Singh, J. Xiao, H. Marbach, H.-P. Steinrück, O. Lytken, *Chem. Eur. J.* **2014**, *20*, 8948–8953.

20. a) F. Buchner, K. Flechtner, Y. Bai, E. Zillner, I. Kellner, H.-P. Steinrück, H. Marbach, J. M. Gottfried, *J. Phys. Chem. C* **2008**, *112*, 15458–15465; b) F. Buchner, I. Kellner, W. Hieringer, A. Gorling, H.-P. Steinrück, H. Marbach, *Phys. Chem. Chem. Phys.* **2010**, *12*, 13082–13090.

21. W. Auwärter, K. Seufert, F. Klappenberger, J. Reichert, A. Weber-Bargioni, A. Verdini, D. Cvetko, M. DellAngela, L. Floreano, A. Cossaro, G. Bavdek, A. Morgante, A. P. Seitsonen, J. V. Barth, *Phys. Rev. B* **2010**, *81*, 245403.

22. A. Wiengarten, K. Seufert, W. Auwärter, D. Ecija, K. Diller, F. Allegretti, F. Bischoff, S. Fischer, D. A. Duncan, A. C. Papageorgiou, F. Klappenberger, R. G. Acres, T. H. Ngo, J. V. Barth, *J. Am. Chem. Soc.* **2014**, *136*, 9346 – 9354.

23. P. W. Atkins, J. de Paula, *Elements of Physical Chemistry*, Wiley-VCH, Oxford, **2013**.

24. a) J. Hennig, H.-H. Limbach, J. Chem. Soc. Faraday Trans. 2 1979, 75, 752–766; b) W. Auwärter, K. Seufert, F. Bischoff, D. Ecija, S. Vijayaraghavan, S. Joshi, F. Klappenberger, N. Samudrala, J. V. Barth, *Nat. Nanotechnol.* **2011**, *7*, 41–46; c) M. Schlabach, B. Wehrle, H. Rumpel, J. Braun, G. Scherer, H.-H. Limbach, *Ber. Bunsenges. Phys. Chem.* **1992**, *96*, 821–833; d) J. Braun, M. Köcher,

M. Schlabach, B. Wehrle, H.-H. Limbach, E. Vogel, *J. Am. Chem. Soc.* **1994**, *116*, 6593–6604.

25. W. Auwärter, D. Écija, F. Klappenberger, J. V. Barth, *Nat. Chem.* **2015**, *7*, 105–120.

26. I. Horcas, R. Fernández, J. M. Gómez-Rodríguez, J. Colchero, J. Gómez- Herrero, A. M. Baro, *Rev. Sci. Instrum.* **2007**, *78*, 013705.

27. P. Feulner, D. Menzel, *J. Vac. Sci. Technol.* **1980**, *17*, 662–663.

28. M. J. Frisch, G. W. Trucks, H. B. Schlegel, G. E. Scuseria, M. A. Robb, J. R. Cheeseman, G. Scalmani, V. Barone, B. Mennucci, G. A. Petersson, H. Nakatsuji, M. Caricato, X. Li, H. P. Hratchian, A. F. Izmaylov, J. Bloino, G. Zheng, J. L. Sonnenberg, M. Hada, M. Ehara, K. Toyota, R. Fukuda, J. Hasegawa, M. Ishida, T. Nakajima, Y. Honda, O. Kitao, H. Nakai, T. Vreven, J. A. Montgomery Jr. , J. E. Peralta, F. Ogliaro, M. Bearpark, J. J. Heyd, E. Brothers, K. N. Kudin, V. N. Staroverov, R. Kobayashi, J. Normand, K. Raghavachari, A. Rendell, J. C. Burant, S. S. Iyengar, J. Tomasi, M. Cossi, N. Rega, N. J. Millam, M. Klene, J. E. Knox, J. B. Cross, V. Bakken, C. Adamo, J. Jaramillo, R. Gomperts, R. E. Stratmann, O. Yazyev, A. J. Austin, R. Cammi, C. Pomelli, J. W. Ochterski, R. L. Martin, K. Morokuma, V. G. Zakrzewski, G. A. Voth, P. Salvador, J. J. Dannenberg, S. Dapprich, A. D. Daniels, Ö. Farkas, J. B. Foresman, J. V. Ortiz, J. Cioslowski, D. J. Fox, in Gaussian 09W, Gaussian Inc., Wallingford CT, **2009**.

29. J. P. Perdew, K. Burke, M. Ernzerhof, *Phys. Rev. Lett.* **1996**, *77*, 3865–3868.